Exposure-based sequence learning induces backward replay in the human visual cortex

Tao He[1,2], Xizi Gong[1,2], Qian Wang[1,2], Xinyi Zhu[1,2], Yunzhe Liu[3,4], Fang Fang[1,2,5,6*]

[1] School of Psychological and Cognitive Sciences and Beijing Key Laboratory of Behavior and Mental Health, Peking University, Beijing 100871, People's Republic of China

[2] IDG/McGovern Institute for Brain Research, Peking University, Beijing 100871, People's Republic of China

[3] State Key Laboratory of Cognitive Neuroscience and Learning, IDG/McGovern Institute for Brain Research, Beijing Normal University, Beijing, People's Republic of China.

[4] Chinese Institute for Brain Research, Beijing, People's Republic of China.

[5] Peking-Tsinghua Center for Life Sciences, Peking University, Beijing 100871, People's Republic of China

[6] Key Laboratory of Machine Perception (Ministry of Education), Peking University, Beijing 100871, People's Republic of China

Corresponding author:

Fang Fang, Ph.D. Professor

School of Psychological and Cognitive Sciences

Executive Associate Director, IDG/McGovern Institute for Brain Research

Peking University

5 Yiheyuan Road, Beijing 100871, P. R. China

Phone: +86-10-62756932

Email: ffang@pku.edu.cn

Web: http://www.psy.pku.edu.cn/english/people/faculty/professor/fangfang/index.htm

ABSTRACT

The brain demonstrates a sustained capacity for cortical plasticity, as extensively studied in task-dependent training contexts. However, the cortical plasticity induced by exposure-based learning has been largely ignored despite its potential significance in promoting generalization and adaptability, thereby allowing individuals to effortlessly apply their knowledge across diverse tasks. One of the key mechanisms underlying the cortical plasticity induced by learning is the replay of learned events, as originally described for rodents and recently identified in humans. In the current study, we recorded magnetoencephalography (MEG) signals to investigate the relationship between exposure-based sequence learning and replay in the human brain. Participants were exposed to a predefined sequence of four motion directions for 30 min, and subsequently presented with start/end motion direction of the sequence as a cue aiming to induce replay of the motion sequence. During the post-cue blank period, we observed a backward replay of the motion sequence in a time-compressed manner. These effects were marginally significant even for a very brief exposure. However, when we flashed the second or third motion direction of the sequence as a cue, no replay events were observed. Further analyses revealed that activity in the medial temporal lobe (MTL) preceded the ripple power in the visual cortex at replay onset, implying a potentially coordinated relationship between the activity in the MTL and visual cortex. Taken together, our study demonstrated the rapid development of replay events induced by simple visual exposure in humans, providing new insights into the mechanisms underlying cortical plasticity even without explicit training tasks.

INTRODUCTION

The capacity of cortical circuits to undergo structural and functional plasticity in response to experience is a fundamental characteristic of the brain, extending beyond the critical period of development [1–3]. To date, cortical plasticity has been studied in association with various forms of learning, primarily within task-dependent training contexts. For example, training to discriminate or identify visual patterns (i.e., visual perceptual learning, VPL) has been shown to refine the neural representations of trained stimuli in the visual cortex and optimize the connections or weights between visual and decision-making cortical areas [4–6]. Learning motor-related procedures (e.g., juggling, piano playing) produces microstructural changes in both the white [7] and gray matter [8].

Despite extensive cortical plasticity studies on task-dependent learning, little attention has been paid to task-independent, or exposure-based learning. Exposure-based learning, which occurs through repeated exposure to a stimulus, has been shown to impact the perception of sensory information and facilitate the prediction of upcoming stimuli [9–11]. This form of learning promotes generalization and adaptability, allowing individuals to effortlessly apply their knowledge across diverse tasks. Indeed, a previous study revealed that after exposing to oriented stimuli at unattended locations, discrimination performance improvement occurs not only with the exposed oriented stimuli, but also with complex stimuli (e.g., natural images) containing the exposed orientations, suggesting a robust generalization in exposure-based learning [9]. However, our understanding of the neural mechanisms of exposure-based learning is still quite

limited, though few studies have shown that it could alter the strength and selectivity of neuronal responses in visual cortex [12–14].

One of the most recent and remarkable findings related to human cortical plasticity is learning-induced replay. Replay refers to the sequential reactivation of neural activity patterns associated with prior experience. During replay, the neural representations of a past experience can be compressed in time [15–19]. These replay events frequently coincide with sharp-wave ripples (SWRs), which are high-frequency (150–220 Hz) ripple oscillations [20,21] observed in the local field potential [22,23] associated with learning processes [24–26]. Thus far, existing studies exclusively focused on replay induced by sequence learning within task-dependent contexts. For instance, in reinforcement learning, a backward sequential replay was associated with nonlocal reinforcement learning processes [27] and in episodic learning, a fast sequential replay of episode elements was detected during memory retrieval [28]. However, the relationship between replay and exposure-based sequence learning in the human brain remains unknown.

In the current study, we used magnetoencephalography (MEG) to investigate the properties of replay events induced by sequence exposure in the human brain. Herein, the participants were exposed to a predefined motion sequence for approximately 30 min (i.e., pre-exposure). Immediately thereafter, we presented the first (start-only condition) or last (end-only condition) motion direction as a cue in a trial, and these trials mixed with full sequence trials that served as topping-up exposure. Temporally delayed linear modeling [29] was applied to the MEG signals to capture the temporal sequence of internally generated neural representations of motion directions. During the post-cue

blank period, we found a time-compressed, cue-triggered backward replay of the previously exposed motion sequence in the visual cortex, regardless whether the start or end cue was presented. We detected this effect even without pre-exposure. However, neither a forward nor a backward replay of the motion sequence was detected when flashing an intermediate motion direction (i.e., 2nd or 3rd motion direction in the sequence) as a cue. Finally, we performed MEG source reconstruction analysis; the results showed that MTL activation preceded visual cortical activation, suggesting that the replay events observed in the visual cortex may be triggered by activities in the MTL.

RESULTS

The current study consisted of three MEG experiments. In each experiment, participant completed two successive phases: the functional localizer phase and the exposure-based learning phase. The first was used to train models to decode each motion direction in the sequence. During this phase, one of the four motion directions (0°, 90°, 180°, and 270°) was randomly presented in each trial. The functional localizer was implemented prior to exposure-based learning to prevent any potential contamination of our localizer data by sequence information.

The exposure-based learning phase consisted of pre-exposure and a test, as depicted in Figure 1C. During pre-exposure, the participants were exposed to a fixed sequence of four random-dot kinematograms (RDKs) in the center of the screen for approximately 30 min (full sequence condition, Figure 1A). During the test, we included 50%, 25%, and 25% of full sequence, start-only, and end-only trials, respectively. The full sequence trials served as topping-up exposure to maintain the learning effect. In the

start-only or end-only trials, the first or last RDK of the sequence was presented at the beginning of the trial, followed by a blank period (Figure 1A). We thereafter attempted to characterize the temporal sequence of the internally generated representations of the four RDKs from MEG occipital signals during the blank period. The results showed sequence-evoked responses following the onset of the first RDK in the full sequence trials (Figure 1B, blue line). Remarkably, start-only and end-only trials elicited similar wave-like responses as the full sequence trials (Figure 1B, yellow and green lines), resembling the results of a previous fMRI study that demonstrated cue-triggered anticipatory evoked responses in V1 [30].

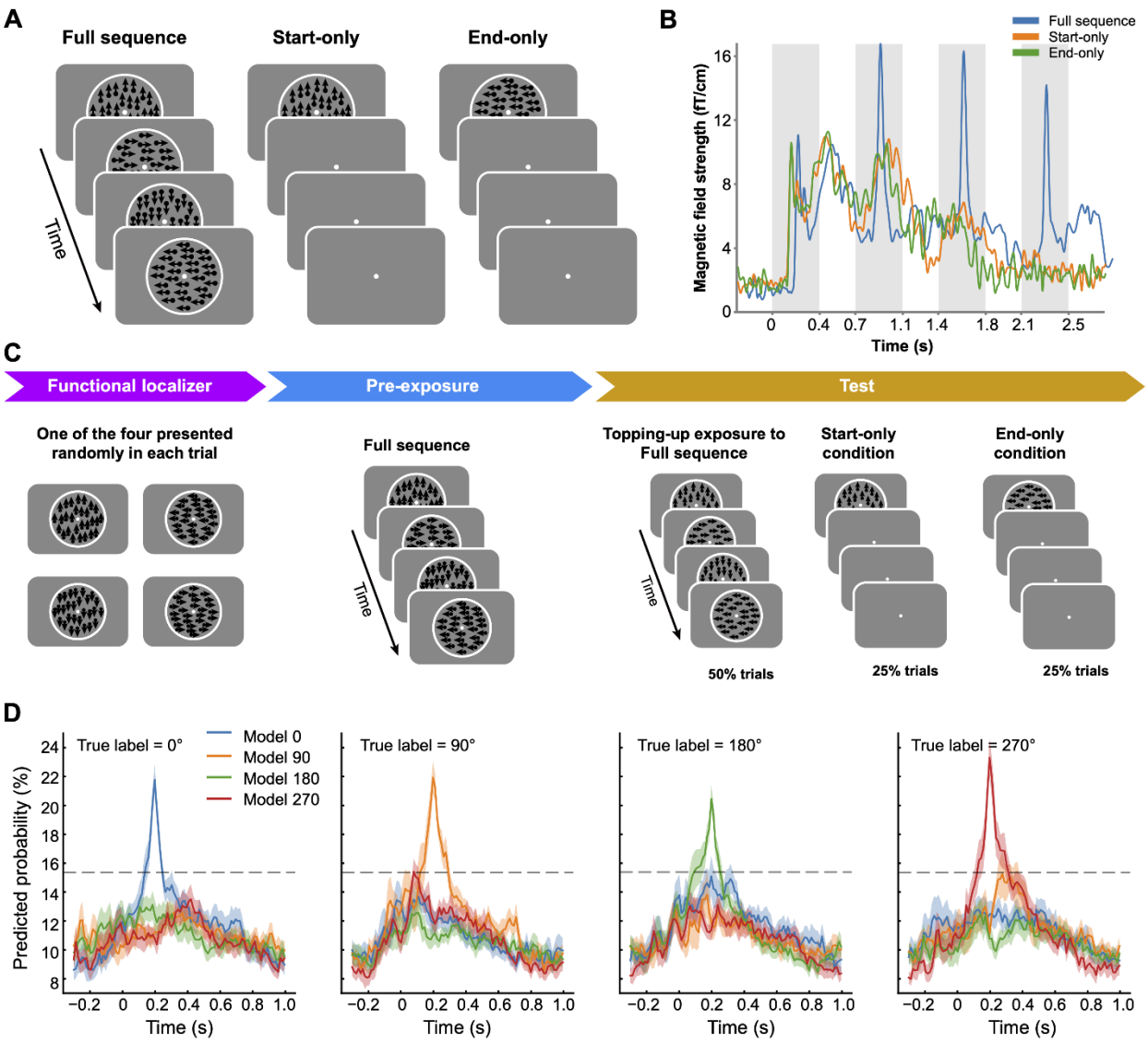

Figure 1. Stimuli, experimental procedure, and classifier performance in Experiment 1

(A) Participants were presented with random-dot kinematograms (RDKs) in three conditions, the full sequence, start-only, and end-only conditions. In 10% of full sequence trials, participants were asked to detect a speed change in one of the four RDKs. **(B)** Evoked responses as a function of time relative to trial onset in the full sequence (blue line), start-only (yellow line), and end-only (green line) conditions, respectively. **(C)** During MEG scanning, participants were presented with two functional

localizer runs before providing any sequence information. Next, four full sequence runs served as pre-exposure. Finally, in the test, full sequence, start-only and end-only trials were presented in a pseudo-randomized order. Here, full sequence trials served as topping-up exposure. **(D)** The predicted probabilities were aligned at 200 ms post-stimulus onset according to their corresponding optimal time point per participant and motion direction. Each colored line indicates the predicted results of a decoding model applied to a motion direction dataset. The dashed horizontal line indicates the permutation threshold estimated by random shuffling of the labels and re-decoding.

Construction of decoding models of motion directions

To index cue-evoked replay in the visual cortex throughout the post-cue blank period in each trial, we first developed four decoding models using functional localizer data to capture the neural features of the four motion directions in the RDKs. For each participant, we trained a one-versus-rest Lasso logistic regression model to identify the neural activity pattern elicited by each motion direction. MEG signals from 72 occipital sensors were selected as features in the training model. We used a leave-one-out cross-validation scheme on localizer data to independently estimate the decoding accuracy at each time point (Figure S1A). At the group level, decoding accuracies peaked at 411 ms, 464 ms, 444 ms, and 434 ms after stimulus onset for motion directions 0° (55.37% ± 1.21), 90° (58.10% ± 1.14), 180° (54.07% ± 1.47), and 270° (53.64% ± 1.34), respectively. There were no significant differences among the four motion directions in terms of either latency ($F(3, 51) = 0.375$, $p = 0.7716$, $\eta_p^2 = 0.0159$) or decoding accuracy ($F(3, 51) = 2.757$, $p = 0.0517$, $\eta_p^2 = 0.091$) at the peak time point.

We selected the time point with the highest decoding accuracy as the optimal time point for each participant and motion direction, as these time points are believed to carry the richest feature information [31]. For subsequent analyses, we used classifiers trained at their respective optimal time point. Finally, we obtained four classifiers, each yielding significant prediction probabilities only when the stimulus matched the motion direction that the classifier was trained to detect (Figure 1D). We did not find any spatial correlation between any two trained classifiers (highest correlation $r < 0.12$, Figure S2A). Since each participant and motion direction had an optimal time point at different latencies, we circularly shifted the prediction probability over time and aligned their optimal time points to an arbitrary time point (here, 200 ms post-stimulus onset) for each participant and motion direction, respectively (Figure 1D).

Backward replay of exposed sequence triggered by start and end cue

Having established the decoding models for each participant and motion direction based on the functional localizer data, we then applied the trained decoders to the MEG signals during the post-cue blank period in the start- and end-only conditions to estimate the reactivation probability for each motion direction at each time point [17,28,32]. Example trials for the start- and end-only conditions are shown in Figure S1A. Next, we applied temporally delayed linear modeling (TDLM) to quantify the evidence of sequential replay of motion directions in start- and end-only conditions (Figure 2C). This algorithm includes two-level regression analyses; a first-level regression that quantifies the evidence for each pairwise state-to-state transition, and a second-level regression that evaluates the extent to which the reactivation patterns align with a particular order

of interest. Finally, we defined “sequenceness” as a metric of forward (i.e., 1 → 2 → 3 → 4) or backward (i.e., 4 → 3 → 2 → 1) replay [17,29,32,33].

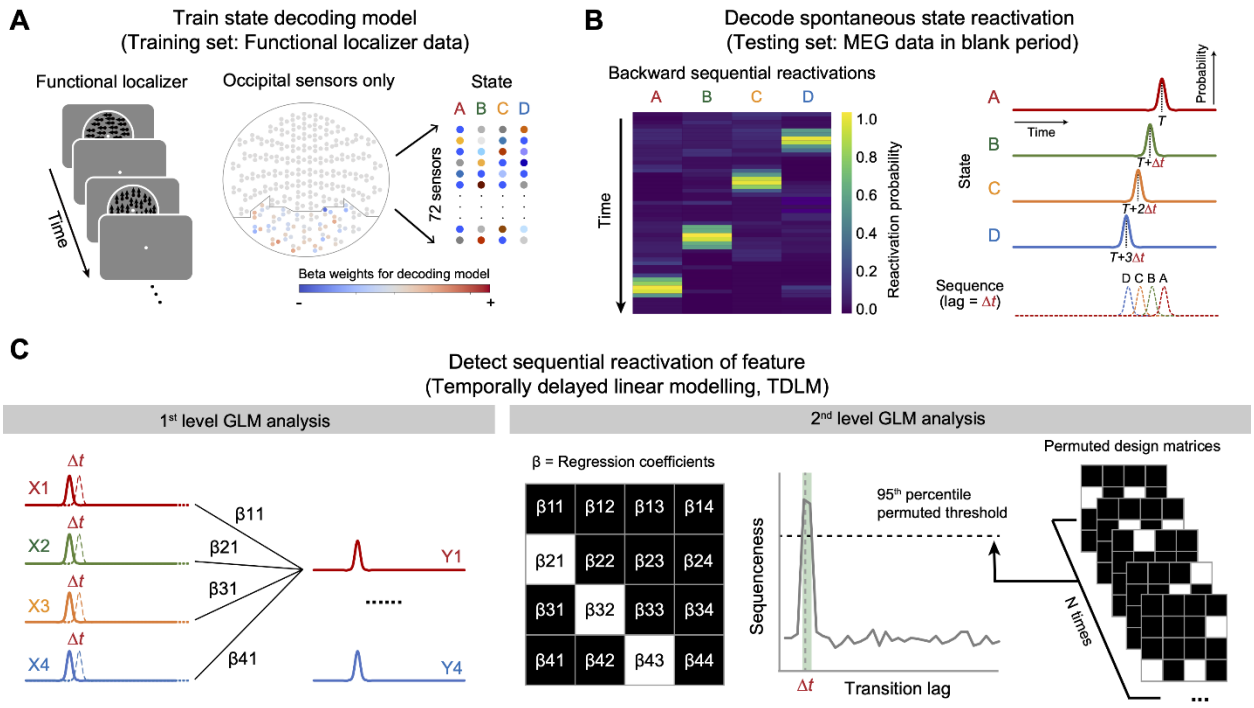

Figure 2. Illustration of replay analysis pipeline: Temporally delayed linear modeling (TDLM)

(A) Regression models were trained for each participant and motion direction using magnetoencephalography (MEG) signals from the occipital sensors acquired in the functional localizer. **(B)** Peak-accuracy classifiers were next applied to MEG signals from the post-cue blank period to derive a decoded [time x state] reactivation matrix. An example of backward sequential reactivation of stimulus is shown on the left. **(C)** Using TDLM, we quantified the evidence that spontaneous neural reactivations follow the order of the exposed visual experience. We initially performed a time-lagged regression to create a regression coefficient matrix [states x states] for each time lag by regressing each lagged predictor matrix X(Δt) onto the state reactivation matrix, Y (i.e., 1st level

GLM analysis). The degree to which the reactivations systematically follow a transition matrix of interest was measured by “sequenceness” (B, right; 2nd level GLM analysis). We tested the magnitude of this effect at each time lag independently for all transition lags up to 600 ms. The dashed line represents the corrected nonparametric statistical significance threshold (see Methods for details). Colored areas indicate the lags when the evidence of sequenceness in the backward direction exceeded the permutation threshold.

In the start-only condition, we found evidence of backward replay of the exposed motion sequence during the post-cue blank period, with a peak transition lag at 28–40 ms (maximal effect at 32 ms-lag: $\beta = -0.0202 \pm 0.002$, $p < 1/24 \approx 0.042$, peak-level significance threshold derived from a nonparametric permutation test, family-wise error (FWE) corrected across lags, Figure 3B). Figure 3A shows an example of backward sequential reactivation, found in most participants (Figure S3A). In the end-only condition, we also found evidence of backward replay events during the post-cue blank period, with a peak transition lag at 28–36 ms (maximal effect at 32 ms-lag: $\beta = -0.0145 \pm 0.0016$, $p < 1/24 \approx 0.042$, peak-level significance threshold obtained from a nonparametric permutation test, FWE corrected across lags; Figure 3D). Figure 3C shows an example of backward sequential reactivation in this condition. This effect was also observed in most participants (Figure S3A). In a control analysis, we conducted a comprehensive examination of all 24 potential sequences. Our findings confirmed that only backward sequential reactivations (specifically, sequence 4 → 3 → 2 → 1) exhibited significant results in both start-only and end-only conditions (Figure S4).

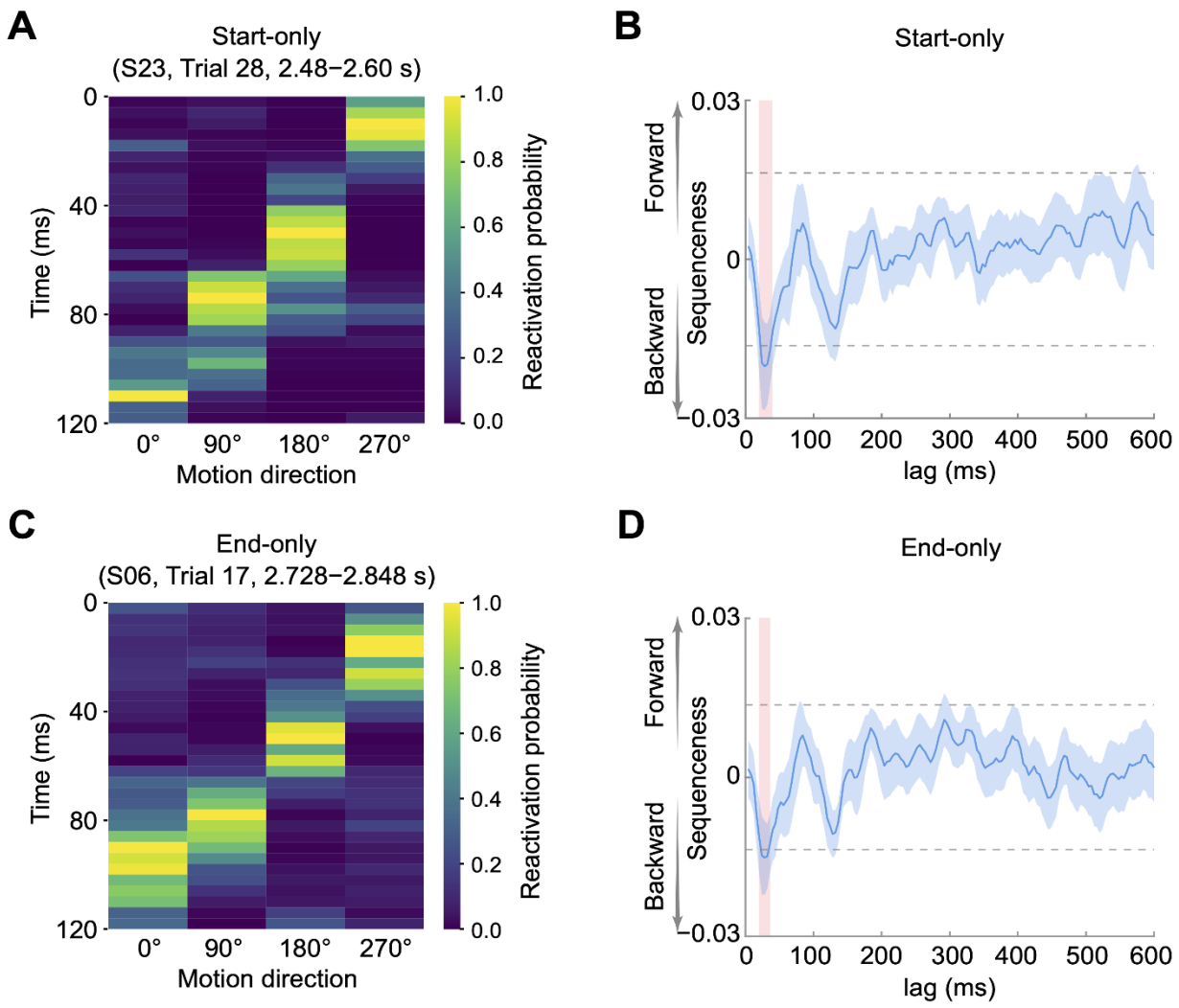

Figure 3. Backward replay in both start- and end-only conditions

(A and **C)** Example of backward sequential reactivation in the start- (A) and end- (C) only conditions for a representative participant. Each row represents the reactivation probability at that time point and each column indicates the motion direction. **(B)** Backward replay of the exposed motion sequence with peak transition lags at 28–40 ms in the start-only condition. Horizontal dashed lines represent corrected significance levels from a nonparametric permutation test at the 2nd-level GLM analysis of TDLM. **(D)** Backward replay with peak transition lags at 28–36 ms in the end-only condition. Horizontal dashed lines indicate the same as in (B).

Backward replay is cue-dependent and depends on the amount of exposure

Next, we explored whether the replay events observed in Experiment 1 were cue independent. Specifically, whether the sequential reactivation of neural response patterns would occur regardless the element of the sequence presented as a cue. Thus, we conducted Experiment 2, similarly to Experiment 1 but with a different cue. Instead of flashing the first or last RDK, we presented the second or third RDK as cue (2nd-only or 3rd-only condition, see Figure S5A and Methods). Our hypothesis was that if the start and end points of the sequence were particularly important for replay formation, presenting a non-terminal cue would unlikely induce replay during the post-cue period. The evoked responses for all conditions in Experiment 2 are shown in Figure S5B, and the robust classifiers for each motion direction are shown in Figure S5C. There was no evidence of either forward or backward replay in either condition (maximal nonsignificant effect at 32 ms-lag: 2nd-only condition, $\beta = -0.0024 \pm 0.0014$; 3rd-only condition, $\beta = -0.0018 \pm 0.0015$; Figure 4A).

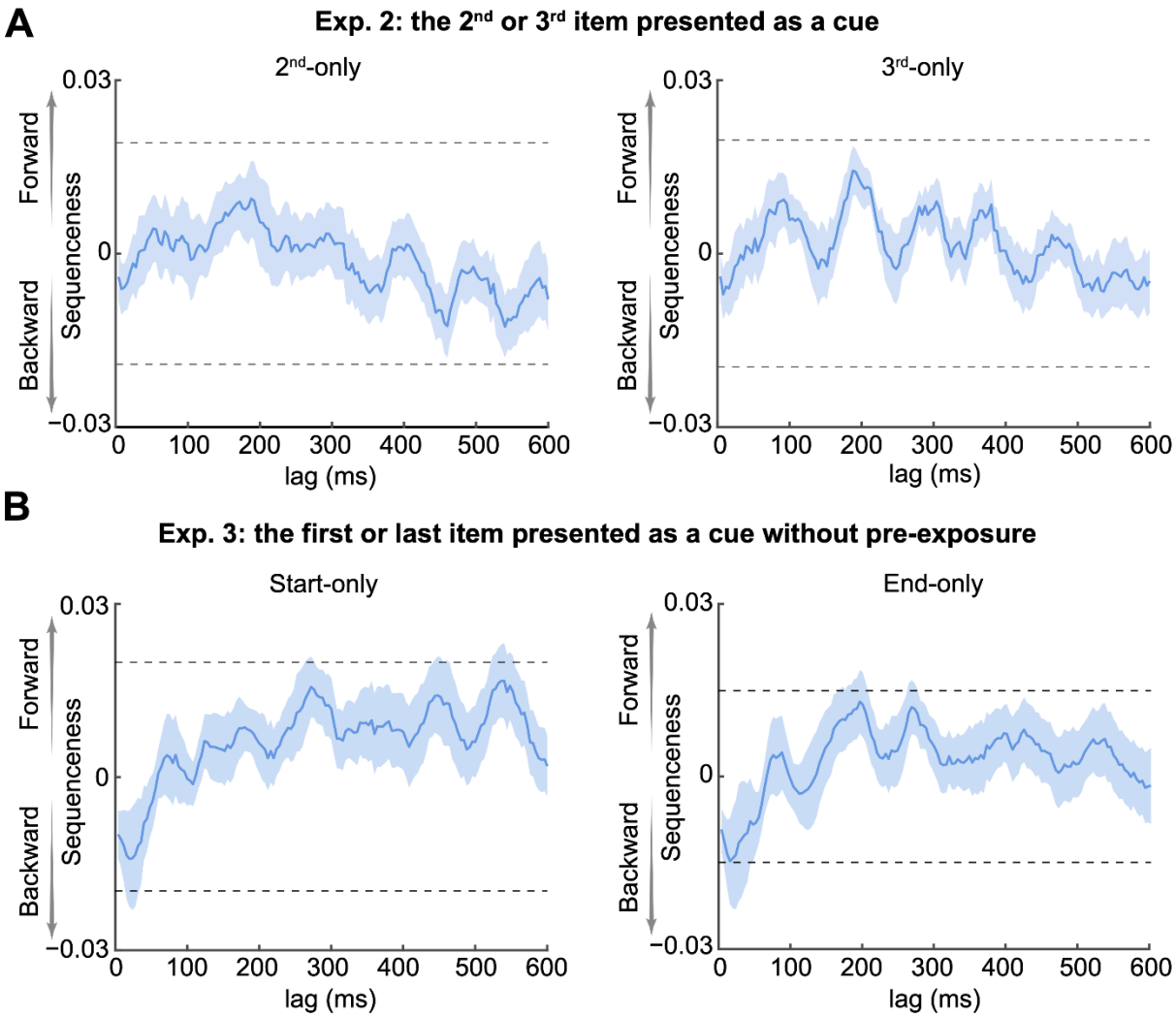

Figure 4. Backward replay is cue-dependent and depends on the amount of exposure

(A) No evidence for replay was found in either the 2nd-only (left) or 3rd-only condition in Experiment 2 (right). Horizontal dashed lines correspond to those in Figure 3B and D. **(B)** In Experiment 3, participants were exposed to full sequence (i.e., topping-up exposure), start-only and end-only trials without pre-exposure. In the end-only condition, there was backward replay; however, in the start-only condition, no such replay was observed.

Finally, we investigated how changing the amount of exposure would affect replay events during the blank period. To address this question, we conducted Experiment 3, also similar to Experiment 1 except for the removal of pre-exposure. Accordingly, only 50% of full sequence trials in the test served as “topping-up” exposure. The results of evoked responses and trained classifiers in Experiment 3 are shown in Figure S6. In the start-only condition, we found a numerical trend of backward replay at transition lags at 20–40 ms, although it did not reach statistical significance (maximum effect at 28 ms-lag: $\beta = -0.0139 \pm 0.0021$). In the end-only condition, the evidence of backward replay just reached the significance level at transition lags at 20–40 ms (maximal effect at 24 ms-lag: $\beta = -0.0147 \pm 0.0019$, $p < 1/24 \approx 0.042$, using the peak-level significance threshold from a nonparametric permutation test, FWE-corrected across lags; Figure 4B).

Power increase in replay-associated sharp-wave ripple frequencies

Previous studies on rodents and humans showed that replay events were associated with increased high-frequency ripple power [23,32]. To investigate whether such a pattern of replay-associated power increase could be observed in our study, we performed a time-frequency analysis using combined data from the start-only and end-only conditions. First, we identified putative replay onsets during the post-cue blank period in each trial, using probabilities decoded from MEG signals in the occipital region. Next, replay onsets were determined by choosing time points with a high (>95th percentile) probability for backward sequential reactivations with a 32 ms-lag transition (maximal replay effect at the group level for both start- and end-only conditions, Figure

3B and D; see Methods for details). Finally, using the MEG signals obtained from whole brain sensors, we found a transient increase in ripple power at 120–160 Hz at the onset of replay events, compared to a baseline period of 50–100 ms prior to replay onset (Figure 5A; cluster-based permutation test with cluster forming threshold t > 3.1 and 5000 permutations).

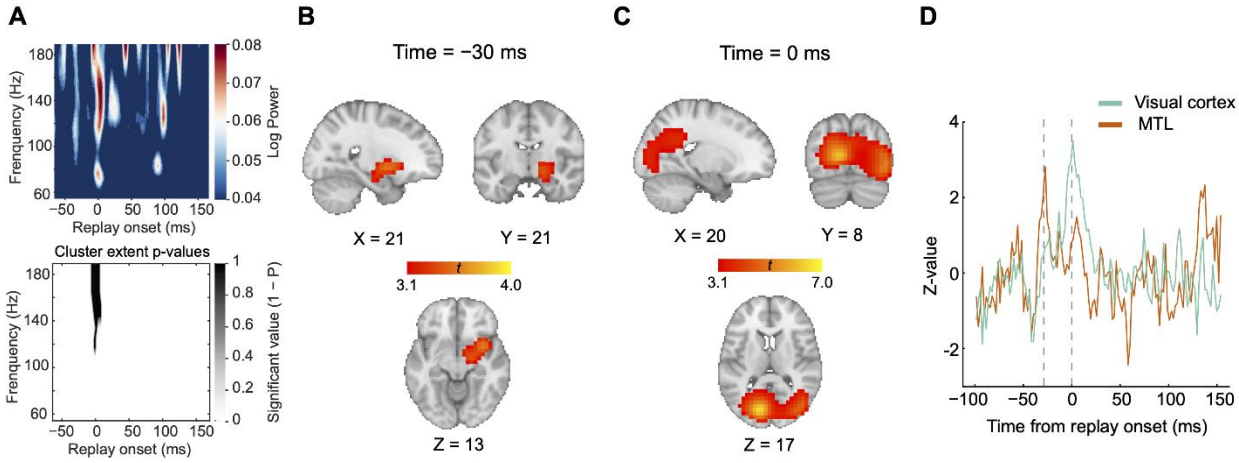

Figure 5. Replay events align with ripple power, with source activation in the MTL preceding activation in the visual cortex

(A) Top: In Experiment 1, a time-frequency decomposition of sensor-level data revealing a brief increase in high-frequency oscillatory power at replay onsets. Bottom: a cluster-based permutation test (cluster forming threshold, t > 3.1; number of permutations = 5000) could identify a significant cluster around 140 Hz. **(B)** Source localization of ripple-band power 30 ms before replay onsets showing significant activation in the MTL (peak Montreal Neurological Institute [MNI] coordinates: X = 21, Y = 21, Z = 13. Neurological orientation.) **(C)** Source localization of ripple-band power at replay onsets showing significant activation in the visual cortex (peak MNI coordinates: X = 20, Y = 8, Z = 17). **(D)** The activation time course of the MTL at its peak MNI

coordinate is shown in red, whereas that of the visual cortex at its peak MNI coordinate is displayed in green. The MTL reached its peak activation before the visual cortex.

Visual cortical activation lags MTL activation

Since replay events were obtained using decoding probabilities from only 72 occipital sensors, it is highly possible that replay events also occurred in the visual cortex. Therefore, we next examined whether our observed replay onsets were related to power increases within the visual cortex. Using a linearly constrained minimum variance (LCMV) beamforming algorithm [34], we first epoched the data using replay onsets combined from both the start-only and end-only conditions and then beamformed the broadband power into the source space (see Methods for details). We found that the power increase at replay onsets was localized to sources in the bilateral visual cortex (Figure 5C). Particularly, the right MTL, including the hippocampus and amygdala, was associated with power increases prior to the onset of replay events (Figure 5B). Specifically, activation (i.e., power increase) in the MTL occurred 30 ms (Figure 5B) earlier than that in visual cortex ($p < 0.05$, corrected, whole brain nonparametric permutation test). Finally, for display purposes, we extracted activations from the 10 most activated voxels within the MTL and visual cortex, respectively, and plotted the corresponding time courses of their broadband power. Peak activation in the visual cortex at replay onsets was preceded by peak activation in the MTL (Figure 5D), implying an information flow from the MTL to the visual cortex.

DISCUSSION

Our study revealed a robust backward replay of the exposed motion sequence in the visual cortex. This backward replay could be only reliably triggered by the first or last motion stimulus in the sequence. Intriguingly, after removing pre-exposure, even brief exposure could induce a trend for the replay. We also found that the ripple power in the visual cortex at the replay onset was preceded by that in the MTL. These findings show, for the first time, a replay induced by exposure-based learning in the human visual cortex, which might be initiated by MTL activity.

Learning-induced replay serves as a pivotal cortical plasticity mechanism to support various cognitive functions. Although previous studies have attempted to elucidate the properties of replay in humans, they exclusively focused on the hippocampus within task-dependent training contexts [18,19,35]. Here, we unveiled replay events in the human visual cortex through exposure-based sequence learning. In contrast to the belief that the occurrence of replay requires lengthy task-dependent training, our findings provide two breakthroughs. First, explicit task training is not necessary, as exposure alone is sufficient to induce replay. Second, the exposure does not need to be prolonged, as even a short exposure can elicit replay. In line with our findings, a rodent study detected replay in the hippocampus even after a single experience [36].

Our findings suggest an active communication between the hippocampus and the visual cortex for the occurrence of replay events. Previous studies on memory consolidation considered the exchange of information between these two regions critical

for facilitating replay events through hippocampal-neocortical circuits [15,37–40]. Functionally, replay events offer a mechanism for transferring recent experiences from the hippocampus to the cortex, enabling the encoding of stimulus relationships [41–44]. Further, the current results are consistent with the hypothesis that the hippocampus encodes relationships among stimuli whereas the visual cortex primarily acts as a platform for the manifestation of replay events [45].

How is exposure-based sequence learning implemented through hippocampus-dependent replay in the visual cortex? Three key processes are considered here. First, the hippocampus is involved in learning relationships among stimuli [46–49]; in fact, the ability to learn such relationships drastically decreases when the hippocampus is damaged [50–54]. A recent fMRI study also showed that hippocampal representations are shaped as a successor representation-like predictive map, prioritizing future over past sequence locations to guide future event prediction [55]. Second, visual cortical areas act as a “cognitive blackboard” where task-relevant features are highlighted through feedback connections [56]. Such a blackboard can be flexibly written or edited. Third, there are strong bidirectional connections between the hippocampus and sensory cortices. [57,58]. As proposed by the hippocampal-cortical backward projection model [59], sequential reactivations initially generated in the hippocampus can be quickly and accurately sent back to the sensory cortices, consistent with the findings of [39]. A recent study also provided direct evidence that visual sequence plasticity is impaired when the hippocampus is damaged [51], supporting the hypothesis of functional feedback information flow.

Our finding of backward replay in the visual cortex raises another interesting question: why does it manifest in a reverse order? To date, there is no consensus on this issue. In rodents, a seminal study of replay during the awake state showed that when animals stopped at the end of a rewarded pathway, place cells were reactivated in the reverse order of the previously experienced direction [60]. However, a later study revealed that awake replay could occur in either a forward or backward direction relative to behavioral experience [61]. Similarly, in humans, both directions have been observed in different nonspatial cognitive tasks [27,28,32]. Forward replay may be associated with planning [62,63], providing information pertaining to the assessment of future pathways [61]. Backward replay may be more related to learning, as often observed at the end of runs when animals consume a reward [60,64]. Nevertheless, the exact function of the replay direction remains mysterious, as both forward and backward replays are modulated by task demands [65]. Thus, the underlying neural mechanisms of backward replay in the visual cortex remain to be investigated.

Finally, we also found that replay occurrence is modulated by the cue. This result highlights the importance of the start and end points of the sequence in the replay. One fascinating proposal is that the replay event is sensitive to sequence boundaries, as indicated by the role of the start or end point of the sequence as salient boundaries that anchor place cell firing [66]. Accordingly, previous studies have shown that when rats are trained to run along a linear track starting at different points, place fields tend to be anchored to either the start or end of the journey [67,68], suggesting that a boundary is essential to sequence integrity and may play a pivotal role in triggering replay onset. An alternative explanation to these findings posits that the onset of the second or third

stimuli in the sequence might reinstate the neural representations of a partial visual sequence. For example, for a given sequence, A → B → C → D, flashing the third stimulus (i.e., C) might only trigger a backward reactivation of the sequence giving C → B → A during the blank period.

In conclusion, our results showed that exposure-based sequence learning can lead to backward replay events in the visual cortex. These events, occurring in a time-compressed manner, are elicited by the start or end point of the sequence. Replay events might be implemented through the hippocampal-neocortical system. This study broadens our understanding of replay events as a key mechanism of cortical plasticity. The replay occurs not only in the hippocampus but also in the visual cortex and not only in task-dependent, but also exposure-based contexts.

METHODS

Participants

A total of 59 healthy participants (29 females) were involved in the three experiments (Experiment 1: n = 21, 11 females, 22.1 ± 2.61 years; Experiment 2: n = 18, 10 females, 23.56 ± 3.29 years; Experiment 3: n = 20, 10 females, 20.65 ± 2.62 years). In Experiment 1, data from three participants were excluded before analyses, as two showed large head motion (>20 mm) and the behavioral performance of one was at chance level. In Experiment 3, data from two participants were excluded before analyses because of large head motion (>20 mm). All participants were recruited in exchange for monetary compensation (100 RMB/h). They reported normal or corrected-

to-normal vision and had no history of neurological disorders. They were naive to the purposes of the study. The experiments reported here were carried out in accordance with the guidelines expressed in the Declaration of Helsinki. All participants provided written informed consent in accordance with the procedures and protocols approved by the Human Subject Review Committee of Peking University.

Task

Experiment 1

Visual stimuli were RDKs with 100% coherence. All dots in an RDK moved in the same direction (luminance: 2.86 cd/ m^2; diameter: 0.1°; speed: 8°/s) and were presented against a gray background (luminance: 16.7 cd/m^2). At any one moment, 400 dots were visible within a 9° circular aperture and moved in one of the four directions: 0° (right), 90° (up), 180° (left), and 270° (down). Each participant completed two phases successively in the MEG scanner, namely, the functional localizer phase and the exposure-based learning phase (Figure 1C). In the functional localizer phase, each trial started with the presentation of a RDK for 1 s followed by a 1–1.5 s intertrial interval. Participants did not need to perform any task in this phase. The motion direction of the RDK was randomly chosen from the four directions. Each participant performed two functional localizer runs, each run comprising 100 trials, resulting in a total of 50 trials per motion direction. The localizer data was used to train motion direction classification models; this phase required approximately 10 min.

The exposure-based learning phase consisted of pre-exposure and a test. In pre-exposure, we showed participants the four RDKs in either clockwise or

counterclockwise order (e.g., 0° → 90° → 180° → 270°, Figure 1A and 1C); each was displayed for 400 ms, followed by 300 ms of a blank screen with fixation only. Therefore, the total sequence lasted for 2.8 s. The order was counterbalanced among participants, but once decided, it was fixed for each participant. Participants were instructed to detect an oddball RDK by pressing a button, i.e., in 20% trials, dots in one of the four RDKs traveled at a faster speed (9°/s). Each participant completed four runs of 50 trials.

In the test, participants were presented with trials in three different conditions: full sequence condition (50% trials), start-only condition (25% trials), and end-only condition (25% trials). Trials in the full sequence condition were identical to those in pre-exposure which served as "topping-up" exposure to maintain the learning effect, similar to "topping-up" adaptation in visual adaptation studies [69]. In the start- and end-only conditions; however, we only presented the first RDK (start-only condition) or the last RDK (end-only condition) of the full sequence. For a given run, the order of the three conditions was pseudorandomized with the restriction that the start-only and end-only trials were always preceded or followed by a full sequence trial. Participants performed an identical oddball detection task as during pre-exposure. The oddball occurred in 10% of full sequence trials. Finally, each participant completed four runs of 48 trials, yielding a total of 96 full sequence trials, 48 start-only trials and 48 end-only trials.

Experiments 2 and 3

In Experiment 2, we only presented the second or the third RDK as a cue at the start of the trial (Figure S5A), referred to as the 2nd-only and 3rd-only conditions, respectively. The procedure of Experiment 2 was similar to that of Experiment 1 except

that the start- and end-only conditions were replaced by the 2nd-only and 3rd-only conditions. Experiment 3 followed the same procedure as Experiment 1 except that pre-exposure was removed.

QUANTIFICATION AND STATISTICAL ANALYSIS

MEG acquisition and preprocessing

Neuromagnetic signals were recorded continuously at 1000 Hz with a 306-channel (204 planar gradiometers; 102 magnetometers), whole-head MEG system (Elekta Neuromag TRIUX) in a magnetically shielded room. Before scanning, four-headed position indicator coils attached to the scalp determined the head position with respect to the sensor array. Coil location was digitized with respect to three anatomical landmarks (nasion and preauricular points) with a 3D digitizer (Polhemus Isotrak system). Participants sat upright inside the scanner, while the stimuli were projected onto a screen suspended in front of them. Participants responded using a MEG-compatible button box held in their right hand.

To reduce noise from external environment, the temporal extension of signal-space separation (tSSS) method was applied at the preprocessing stage using the Elekta Neuromag MaxFilter software [70]. MEG signals were high-pass filtered at 0.5 Hz using a first-order IIR filter to remove slow-drifts. Data were then downsampled from 1000 Hz to 250 Hz for sequenceness analysis or 500 Hz for time-frequency analysis. Excessively noisy segments and sensors were automatically removed before independent component analysis (FastICA, http://research.ics.aalto.fi/ica/fastica) and performed to remove artifacts including

cardiac signals, eye movements and blinks, and environmental noise. Artifact components were removed by visual inspection of spatial topography, time course, kurtosis of the time course, and frequency spectrum of all components. MEG epochs from the trial onset were segmented for each trial and baseline-corrected (i.e., subtracting the mean of 300 ms prestimulus baseline from the data) before analyses. Only 72 sensors covering the occipital lobe, labeled as “Occipital” in the MEG data acquisition system were used for all MEG data analyses, except for source localization. The sensor selection was primarily motivated by the main objective of the study, examining functional plasticity (i.e., replay events) in the visual cortex.

Optimal time point of motion direction representation

The optimal time point of motion direction representation was considered as the time point with the highest decoding accuracy. To index the optimal time point of each motion direction for each participant, we conducted time-resolved motion direction decoding analysis on the functional localizer data using Lasso-regularized logistic regression models. A leave-one-trial-out cross-validation procedure was used to train the classifier to determine one of the four motion directions, yielding a decoding accuracy at each time point for each participant. Finally, the time point with the highest decoding accuracy was independently extracted for each participant and each motion direction. These time points are referred to as optimal time points and were used for sequenceness analysis. The optimal time points in Experiment 1 are reported in the Results section. For Experiment 2, at the group level, decoding accuracies peaked at 436 ms, 416 ms, 421 ms, and 442 ms after stimulus onset for motion directions 0°

(54.38% ± 1.70), 90° (52.41% ± 1.44), 180° (51.50% ± 1.11), and 270° (53.40% ± 1.35), respectively. There were no significant differences among the motion directions in terms of latency (F(3, 51) = 0.083, p = 0.9692, η_p^2 = 0.0034) or decoding accuracy (F(3, 51) = 0.9631, p = 0.4173, η_p^2 = 0.0313) at the peak time point. For Experiment 3, at the group level, decoding accuracies peaked at 483 ms, 451 ms, 461 ms, and 499 ms after stimulus onset for motion directions 0° (51.92% ± 1.32), 90° (53.69% ± 1.04), 180° (51.0% ± 1.15), and 270° (53.50% ± 1.54), respectively. There were no significant differences among the motion directions in terms of latency (F(3, 51) = 0.4263, p = 0.7350, η_p^2 = 0.018) or decoding accuracy (F(3, 51) = 1.6207, p = 0.1960, η_p^2 = 0.0411) at the peak time point.

Sequenceness measure

To identify sequenceness during the post-cue blank period in each trial, we trained models to detect transient spontaneous neural reactivation of each feature representation. Therefore, one-versus-rest Lasso-regularized logistic regression models were trained separately for each motion direction using the functional localizer data. MEG signals from the 72 occipital sensors obtained throughout all scanning sessions were used to train the decoding models. For each motion direction, we trained a single binomial classifier, using positive instances from trials in which that feature (i.e., one motion direction) was presented and negative examples from trials in which all other features (i.e., the other three motion directions) were presented, together with an equivalent amount of null data from the period of the 1–1.5 s intertrial interval. Null data were included to reduce the spatial correlation among the classifiers, thereby

concurrently lowering the decoding probabilities for all classifiers during the blank period [17,29]. The sensor distributions of beta estimates and the spatial correlation among the classifiers are shown in Figure S2.

The sequenceness analysis pipeline is illustrated in Figure 2. We first applied trained classifiers with the functional localizer data at the optimal time point to MEG signals at each time point during the blank period, to generate a [time x state] reactivation probability matrix for each trial. The TDLM framework was then used to quantify evidence for sequential reactivations consistent with the inferred task transition structure [17,27,29].

TDLM is a multiple linear regression approach to quantify the extent to which a lagged reactivation time course of state i, ($X(\Delta t)_i$, Δt indicates lag time) can predict the reactivation time course of state j, (X_j). Two steps were included in this pipeline. First, we performed multiple separate regressions using each state's reactivation time course as a dependent variable ($j \in [1: 4]$) and the historical (i.e., time-lagged) reactivation time courses of all states ($i \in [1: 4]$) as predictor variables.

$$X_j = \sum_{i=1}^{4} X(\Delta t)_i * \beta(\Delta t)_{i,j} + C \quad (1)$$

The regression coefficients from Equation 1 quantify the evidence for each empirical state → state reactivation pattern at a given time lag, Δt. For example, $\beta(\Delta t)_{ij}$ is the coefficient capturing the unique variance in X_j explained by $X(\Delta t)_i$. All such first-level coefficients were placed in a lag-specific [4 x 4] empirical transition matrix $\boldsymbol{B}$, representing evidence for all possible state-to-state transitions at a specific lag.

In the second step, we quantified evidence supporting that the empirical (lag-specific) transition matrix, $\boldsymbol{B}$, can be predicted by the sequences of interest, i.e., the exposed motion sequence. All transitions of interest were specified in a model transition matrix (1 for transitions of interest and 0 otherwise), separately for forward (as in the visual experience) (T_F), and backward (opposite to the visual experience) direction (T_B). Then, the strength of all sequences of interest was measured by:

$$\boldsymbol{B} = \sum_{r=1}^{4} Z_r * T_r \qquad (2)$$

where $\boldsymbol{B}$ is the [state x state] empirical transition matrix, T_r is the [state x state] predictor transition matrix (for regressor r), predicting the empirical transitions $\boldsymbol{B}$. We included four predictor matrices: (1) T_F: transitions as in the motion sequence in the forward direction (transitions corresponding to [A → B → C → D]), (2) T_B: transitions opposite to the experience in the backward direction ([D → C → B → A], T_B is the transpose of T_F), (3) T_{auto}: self-transitions to control for autocorrelation ([4 x 4] identity matrix), and (4) T_{const}: a constant matrix to model away the average of all transitions, ensuring that any weight on T_F and T_B was not due to general background neural dynamics.

Z_r is the scalar regression coefficient quantifying evidence for the hypothesized sequences in the empirical transitions, i.e., sequence strength. Note, this estimate of sequence strength is a relative quantity. An estimate of zero for state i to state j, for example, does not mean lack of replay from i → j but no stronger replay of i → j than that of other transitions. Repeating the regression in Equation 2 at each time lag (Δt = 4, 8, 12,..., 600 ms) results in both forward and backward sequence strength as a function of time lag. Shorter lags indicate greater time compression, corresponding to faster speed.

In the current study, sequenceness was defined from the contrast between the evidence for sequential replay of task structure in the forward ([A → B → C → D]) versus backward ([D → C → B → A]) direction (i.e., Z_1–Z_2); thus, removing between-participant variance in the sequential replay per se (which may arise secondary to task engagement and measurement sensitivity [17,29]). Positive sequenceness values indicate

replay in a predominantly forward direction, whereas negative sequenceness values indicate replay in a predominantly backward direction.

For statistical inference, we used nonparametric permutation tests involving all possible permutations of the stimulus labels at the second-level regression, equivalent to permuting the rows and columns together of the transition matrices used to calculate sequenceness. For each permutation, we calculated the peak absolute mean sequence strength over participants and across lags (controlling for multiple comparisons across lags). Sequence strength in unpermuted data was considered significant if its absolute magnitude was >95% of the within-permutation peak.

Identifying replay onsets and analyzing time-frequency

Given that the maximal evidence for replay transitions at the group level was a 32 ms-lag, we next identified replay onsets. Replay onsets were defined as the times when a strong reactivation of one stimulus (e.g., A) was followed by a strong reactivation of the next stimulus (e.g., B) in the sequence, with a 32 ms-lag [17,32]. Specifically, we shifted the reactivation matrix X up to the time lag Δt for the first time with maximal evidence for replay (i.e., 32 ms), obtained X(Δt).

$$Proj = X(\Delta t) \tag{3}$$

We then multiplied X by the transition matrix P; corresponding to the unscrambled sequences: X x P. The transition matrix P defines the mapping between the task state corresponding to column i in X, and column i in Orig. Specifically, column i in Orig is the reactivation time course of the state preceding state i in T.

$$Orig = X * P \tag{4}$$

Next, we multiplied Proj and Orig element-wise, summing over the columns of the resulting matrix; therefore, creating a [time x 1] vector, R, in which each element (i.e., row) indicates the strength of replay with a 32 ms-lag at a given moment in time.

$$R_t = \sum_{i=1}^{4} Orig_{ti} * Proj_{ti} \tag{5}$$

Finally, we identified putative replay event onsets by threshold R at its 95th percentile preceded by a 100 ms pre-onset baseline exhibiting a low probability of replay at each time point.

We then epoched MEG data in the blank period surrounding each onset and computed a frequency decomposition (wavelet transformation) in the time window of −100–150 ms using all sensors. We aimed to find an evidence for the power increase in the high-frequency (120–160 Hz) region of interest at replay onset, compared with a pre-onset baseline (−100–−50 ms from onset), as mentioned in our previous study [32]. Finally, we generated two separate [time x frequency] matrices (i.e., using forward and backward task transition matrices separately) by averaging estimates over sensors and events, capturing the typical spectrally-resolved power change at replay onset.

MEG source reconstruction

We identified the neural sources associated with increased ripple power at putative replay onsets. Forward models were generated based on a single shell using the superposition of basic functions that approximately correspond to the plane

tangential to the MEG sensor array. Linearly constrained minimum variance beamforming [34] was used to reconstruct the epoched MEG data to a grid in MNI space (grid step, 5 mm). The sensor covariance matrix for beamforming was estimated using broadband power data across all frequencies. The baseline activity was the mean neural activity averaged over −100–−50 ms relative to replay onsets. All nonartifactual replay epochs were baseline-corrected at source level. This, we obtained whole-brain results for voxels predicted by participant-specific ripple power at replay onsets. Nonparametric permutation tests were performed on the volume of interest to compute the multiple comparison P values of clusters >10 voxels (whole-brain corrected, cluster-defining threshold; t = 3.1, n = 5000 permutations).

Data and Code availability

Data used to generate the findings of this study will be available upon request (subject to participant consent) to the Lead Contact. TDLM MATLAB Code available at: https://github.com/YunzheLiu/TDLM. Custom computer code will be made available upon request to the Lead Contact.

AUTHOR CONTRIBUTIONS

Conceptualization, T.H., Y.L., and F.F.; Investigation, T.H., Q.W., X.G., and X.Z.; Writing – Original Draft, T.H.; Writing – Review & Editing, T.H., Q.W., X.Z., Y.L., and F.F.

ACKNOWLEDGEMENTS

This study was supported by National Science and Technology Innovation 2030 Major Program (2022ZD0204802), the National Natural Science Foundation of China

(31930053), Beijing Academy of Artificial Intelligence (BAAI), and Science Foundation of Beijing Language and Culture University (supported by “the Fundamental Research Funds for the Central Universities”) (22YBB11, 23YJ220009).

DECLARATION OF INTERESTS

The authors declare no competing interests.

REFERENCES

1. Buonomano, D.V., and Merzenich, M.M. (1998). CORTICAL PLASTICITY: From Synapses to Maps. Annual Review of Neuroscience *21*, 149–186. 10.1146/annurev.neuro.21.1.149.

2. Costandi, M. (2016). Neuroplasticity (MIT Press).

3. Li, W. (2016). Perceptual Learning: Use-Dependent Cortical Plasticity. Annual Review of Vision Science *2*, 109–130. 10.1146/annurev-vision-111815-114351.

4. Roelfsema, P.R., van Ooyen, A., and Watanabe, T. (2010). Perceptual learning rules based on reinforcers and attention. Trends in Cognitive Sciences *14*, 64–71. 10.1016/j.tics.2009.11.005.

5. Watanabe, T., and Sasaki, Y. (2015). Perceptual learning: Toward a comprehensive theory. Annu Rev Psychol *66*, 197–221. 10.1146/annurev-psych-010814-015214.

6. Chen, N., Cai, P., Zhou, T., Thompson, B., and Fang, F. (2016). Perceptual learning modifies the functional specializations of visual cortical areas. Proceedings of the National Academy of Sciences *113*, 5724–5729. 10.1073/pnas.1524160113.

7. Scholz, J., Klein, M.C., Behrens, T.E.J., and Johansen-Berg, H. (2009). Training induces changes in white-matter architecture. Nat Neurosci *12*, 1370–1371. 10.1038/nn.2412.

8. Tavor, I., Botvinik-Nezer, R., Bernstein-Eliav, M., Tsarfaty, G., and Assaf, Y. (2020). Short-term plasticity following motor sequence learning revealed by diffusion magnetic resonance imaging. Human Brain Mapping *41*, 442–452. 10.1002/hbm.24814.

9. Gutnisky, D.A., Hansen, B.J., Iliescu, B.F., and Dragoi, V. (2009). Attention Alters Visual Plasticity during Exposure-Based Learning. Current Biology *19*, 555–560. 10.1016/j.cub.2009.01.063.

10. Baker, R., Dexter, M., Hardwicke, T.E., Goldstone, A., and Kourtzi, Z. (2014). Learning to predict: Exposure to temporal sequences facilitates prediction of future events. Vision Res *99*, 124–133. 10.1016/j.visres.2013.10.017.

11. Pojoga, S.A., Kharas, N., and Dragoi, V. (2020). Perceptually unidentifiable stimuli influence cortical processing and behavioral performance. Nat Commun *11*, 6109. 10.1038/s41467-020-19848-w.

12. Watanabe, T., Náñez, J.E., and Sasaki, Y. (2001). Perceptual learning without perception. Nature *413*, 844–848. 10.1038/35101601.

13. Xu, S., Jiang, W., Poo, M., and Dan, Y. (2012). Activity recall in a visual cortical ensemble. Nature Neuroscience *15*, 449–455. 10.1038/nn.3036.

14. Gavornik, J.P., and Bear, M.F. (2014). Learned spatiotemporal sequence recognition and prediction in primary visual cortex. Nat Neurosci *17*, 732–737. 10.1038/nn.3683.

15. Carr, M.F., Jadhav, S.P., and Frank, L.M. (2011). Hippocampal replay in the awake state: a potential substrate for memory consolidation and retrieval. Nat Neurosci *14*, 147–153. 10.1038/nn.2732.

16. Joo, H.R., and Frank, L.M. (2018). The hippocampal sharp wave–ripple in memory retrieval for immediate use and consolidation. Nat Rev Neurosci *19*, 744–757. 10.1038/s41583-018-0077-1.

17. Nour, M.M., Liu, Y., Arumuham, A., Kurth-Nelson, Z., and Dolan, R.J. (2021). Impaired neural replay of inferred relationships in schizophrenia. Cell *184*, 4315-4328.e17. 10.1016/j.cell.2021.06.012.

18. Liu, Y., Nour, M.M., Schuck, N.W., Behrens, T.E.J., and Dolan, R.J. (2022). Decoding cognition from spontaneous neural activity. Nat Rev Neurosci, 1–11. 10.1038/s41583-022-00570-z.

19. McFadyen, J., Liu, Y., and Dolan, R.J. (2023). Differential replay of reward and punishment paths predicts approach and avoidance. Nat Neurosci *26*, 627–637. 10.1038/s41593-023-01287-7.

20. O'Keefe, J., and Nadel, L. (1978). The hippocampus as a cognitive map (Clarendon Press ; Oxford University Press).

21. Bush, D., Ólafsdóttir, H.F., Barry, C., and Burgess, N. (2022). Ripple band phase precession of place cell firing during replay. Current Biology *32*, 64-73.e5. 10.1016/j.cub.2021.10.033.

22. Buzsáki, G. (1986). Hippocampal sharp waves: Their origin and significance. Brain Research *398*, 242–252. 10.1016/0006-8993(86)91483-6.

23. Buzsáki, G. (2015). Hippocampal sharp wave-ripple: A cognitive biomarker for episodic memory and planning. Hippocampus *25*, 1073–1188. 10.1002/hipo.22488.

24. Jadhav, S.P., Kemere, C., German, P.W., and Frank, L.M. (2012). Awake Hippocampal Sharp-Wave Ripples Support Spatial Memory. Science *336*, 1454–1458. 10.1126/science.1217230.

25. Nokia, M.S., Mikkonen, J.E., Penttonen, M., and Wikgren, J. (2012). Disrupting neural activity related to awake-state sharp wave-ripple complexes prevents hippocampal learning. Front Behav Neurosci *6*, 84. 10.3389/fnbeh.2012.00084.

26. Fernández-Ruiz, A., Oliva, A., Fermino de Oliveira, E., Rocha-Almeida, F., Tingley, D., and Buzsáki, G. (2019). Long-duration hippocampal sharp wave ripples improve memory. Science *364*, 1082–1086. 10.1126/science.aax0758.

27. Liu, Y., Mattar, M.G., Behrens, T.E.J., Daw, N.D., and Dolan, R.J. (2021). Experience replay is associated with efficient nonlocal learning. Science *372*. 10.1126/science.abf1357.

28. Wimmer, G.E., Liu, Y., Vehar, N., Behrens, T.E.J., and Dolan, R.J. (2020). Episodic memory retrieval success is associated with rapid replay of episode content. Nature Neuroscience *23*, 1025–1033. 10.1038/s41593-020-0649-z.

29. Liu, Y., Dolan, R.J., Higgins, C., Penagos, H., Woolrich, M.W., Ólafsdóttir, H.F., Barry, C., Kurth-Nelson, Z., and Behrens, T.E. (2021). Temporally delayed linear modelling (TDLM) measures replay in both animals and humans. eLife *10*, e66917. 10.7554/eLife.66917.

30. Ekman, M., Kok, P., and Lange, F.P. de (2017). Time-compressed preplay of anticipated events in human primary visual cortex. Nat Commun *8*, 15276. 10.1038/ncomms15276.

31. Mo, C., Lu, J., Wu, B., Jia, J., Luo, H., and Fang, F. (2019). Competing rhythmic neural representations of orientations during concurrent attention to multiple orientation features. Nat Commun *10*, 1–10. 10.1038/s41467-019-13282-3.

32. Liu, Y., Dolan, R.J., Kurth-Nelson, Z., and Behrens, T.E.J. (2019). Human Replay Spontaneously Reorganizes Experience. Cell *178*, 640-652.e14. 10.1016/j.cell.2019.06.012.

33. Kurth-Nelson, Z., Economides, M., Dolan, R.J., and Dayan, P. (2016). Fast Sequences of Non-spatial State Representations in Humans. Neuron *91*, 194–204. 10.1016/j.neuron.2016.05.028.

34. Van Veen, B.D., van Drongelen, W., Yuchtman, M., and Suzuki, A. (1997). Localization of brain electrical activity via linearly constrained minimum variance spatial filtering. IEEE Trans Biomed Eng *44*, 867–880. 10.1109/10.623056.

35. Ólafsdóttir, H.F., Bush, D., and Barry, C. (2018). The Role of Hippocampal Replay in Memory and Planning. Current Biology *28*, R37–R50. 10.1016/j.cub.2017.10.073.

36. Berners-Lee, A., Feng, T., Silva, D., Wu, X., Ambrose, E.R., Pfeiffer, B.E., and Foster, D.J. (2022). Hippocampal replays appear after a single experience and incorporate greater detail with more experience. Neuron *110*, 1829-1842.e5. 10.1016/j.neuron.2022.03.010.

37. Buch, E.R., Claudino, L., Quentin, R., Bönstrup, M., and Cohen, L.G. (2021). Consolidation of human skill linked to waking hippocampo-neocortical replay. Cell Rep. *35*, 109193. 10.1016/j.celrep.2021.109193.

38. Buzsáki, G. (1996). The hippocampo-neocortical dialogue. Cereb Cortex *6*, 81–92. 10.1093/cercor/6.2.81.

39. Ji, D., and Wilson, M.A. (2007). Coordinated memory replay in the visual cortex and hippocampus during sleep. Nature Neuroscience *10*, 100–107. 10.1038/nn1825.

40. Ólafsdóttir, H.F., Carpenter, F., and Barry, C. (2016). Coordinated grid and place cell replay during rest. Nat Neurosci *19*, 792–794. 10.1038/nn.4291.

41. Alvarez, P., and Squire, L.R. (1994). Memory consolidation and the medial temporal lobe: a simple network model. Proc Natl Acad Sci U S A *91*, 7041–7045.

42. Dimakopoulos, V., Mégevand, P., Stieglitz, L.H., Imbach, L., and Sarnthein, J. (2022). Information flows from hippocampus to auditory cortex during replay of verbal working memory items. eLife *11*, e78677. 10.7554/eLife.78677.

43. Marr, D., and Brindley, G.S. (1971). Simple memory: a theory for archicortex. Philosophical Transactions of the Royal Society of London. B, Biological Sciences *262*, 23–81. 10.1098/rstb.1971.0078.

44. Redish, A.D., and Touretzky, D.S. (1998). The role of the hippocampus in solving the Morris water maze. Neural Comput *10*, 73–111. 10.1162/089976698300017908.

45. Whittington, J.C.R., Muller, T.H., Mark, S., Chen, G., Barry, C., Burgess, N., and Behrens, T.E.J. (2020). The Tolman-Eichenbaum Machine: Unifying Space and Relational Memory through Generalization in the Hippocampal Formation. Cell *183*, 1249-1263.e23. 10.1016/j.cell.2020.10.024.

46. Garvert, M.M., Dolan, R.J., and Behrens, T.E. (2017). A map of abstract relational knowledge in the human hippocampal–entorhinal cortex. eLife *6*, e17086. 10.7554/eLife.17086.

47. Hsieh, L.-T., Gruber, M.J., Jenkins, L.J., and Ranganath, C. (2014). Hippocampal Activity Patterns Carry Information about Objects in Temporal Context. Neuron *81*, 1165–1178. 10.1016/j.neuron.2014.01.015.

48. Staresina, B.P., and Davachi, L. (2009). Mind the Gap: Binding Experiences across Space and Time in the Human Hippocampus. Neuron *63*, 267–276. 10.1016/j.neuron.2009.06.024.

49. Turk-Browne, N.B., Scholl, B.J., Chun, M.M., and Johnson, M.K. (2009). Neural evidence of statistical learning: efficient detection of visual regularities without awareness. J Cogn Neurosci *21*, 1934–1945. 10.1162/jocn.2009.21131.

50. Chun, M.M., and Phelps, E.A. (1999). Memory deficits for implicit contextual information in amnesic subjects with hippocampal damage. Nat Neurosci *2*, 844–847. 10.1038/12222.

51. Finnie, P.S.B., Komorowski, R.W., and Bear, M.F. (2021). The spatiotemporal organization of experience dictates hippocampal involvement in primary visual cortical plasticity. Current Biology *31*, 3996-4008.e6. 10.1016/j.cub.2021.06.079.

52. Hannula, D.E., Tranel, D., and Cohen, N.J. (2006). The Long and the Short of It: Relational Memory Impairments in Amnesia, Even at Short Lags. J. Neurosci. *26*, 8352–8359. 10.1523/JNEUROSCI.5222-05.2006.

53. Konkel, A., Warren, D., Duff, M., Tranel, D., and Cohen, N. (2008). Hippocampal amnesia impairs all manner of relational memory. Frontiers in Human Neuroscience *2*.

54. Schapiro, A.C., Gregory, E., Landau, B., McCloskey, M., and Turk-Browne, N.B. (2014). The necessity of the medial temporal lobe for statistical learning. J Cogn Neurosci *26*, 1736–1747. 10.1162/jocn_a_00578.

55. Ekman, M., Kusch, S., and de Lange, F.P. (2023). Successor-like representation guides the prediction of future events in human visual cortex and hippocampus. eLife *12*, e78904. 10.7554/eLife.78904.

56. Roelfsema, P.R., and de Lange, F.P. (2016). Early Visual Cortex as a Multiscale Cognitive Blackboard. Annual Review of Vision Science *2*, 131–151. 10.1146/annurev-vision-111815-114443.

57. Eichenbaum, H., Yonelinas, A.R., and Ranganath, C. (2007). The Medial Temporal Lobe and Recognition Memory. Annu Rev Neurosci *30*, 123–152. 10.1146/annurev.neuro.30.051606.094328.

58. Henke, K. (2010). A model for memory systems based on processing modes rather than consciousness. Nat Rev Neurosci *11*, 523–532. 10.1038/nrn2850.

59. Rolls, E.T. (2000). Hippocampo-cortical and cortico-cortical backprojections. Hippocampus *10*, 380–388. 10.1002/1098-1063(2000)10:4<380::AID-HIPO4>3.0.CO;2-0.

60. Foster, D.J., and Wilson, M.A. (2006). Reverse replay of behavioural sequences in hippocampal place cells during the awake state. Nature *440*, 680. 10.1038/nature04587.

61. Diba, K., and Buzsáki, G. (2007). Forward and reverse hippocampal place-cell sequences during ripples. Nat Neurosci *10*, 1241–1242. 10.1038/nn1961.

62. Ólafsdóttir, H.F., Barry, C., Saleem, A.B., Hassabis, D., and Spiers, H.J. (2015). Hippocampal place cells construct reward related sequences through unexplored space. eLife *4*, e06063. 10.7554/eLife.06063.

63. Gillespie, A.K., Maya, D.A.A., Denovellis, E.L., Liu, D.F., Kastner, D.B., Coulter, M.E., Roumis, D.K., Eden, U.T., and Frank, L.M. (2021). Hippocampal replay reflects specific past experiences rather than a plan for subsequent choice. Neuron *109*, 3149-3163.e6. 10.1016/j.neuron.2021.07.029.

64. Ambrose, R.E., Pfeiffer, B.E., and Foster, D.J. (2016). Reverse Replay of Hippocampal Place Cells Is Uniquely Modulated by Changing Reward. Neuron *91*, 1124–1136. 10.1016/j.neuron.2016.07.047.

65. Ólafsdóttir, H.F., Carpenter, F., and Barry, C. (2017). Task Demands Predict a Dynamic Switch in the Content of Awake Hippocampal Replay. Neuron *96*, 925-935.e6. 10.1016/j.neuron.2017.09.035.

66. Rivard, B., Li, Y., Lenck-Santini, P.-P., Poucet, B., and Muller, R.U. (2004). Representation of objects in space by two classes of hippocampal pyramidal cells. J Gen Physiol *124*, 9–25. 10.1085/jgp.200409015.

67. Gothard, K.M., Skaggs, W.E., Moore, K.M., and McNaughton, B.L. (1996). Binding of hippocampal CA1 neural activity to multiple reference frames in a landmark-based navigation task. J. Neurosci. *16*, 823–835. 10.1523/JNEUROSCI.16-02-00823.1996.

68. Redish, A.D., Rosenzweig, E.S., Bohanick, J.D., McNaughton, B.L., and Barnes, C.A. (2000). Dynamics of Hippocampal Ensemble Activity Realignment: Time versus Space. J. Neurosci. *20*, 9298–9309. 10.1523/JNEUROSCI.20-24-09298.2000.

69. Fang, F., Murray, S.O., Kersten, D., and He, S. (2005). Orientation-Tuned fMRI Adaptation in Human Visual Cortex. Journal of Neurophysiology *94*, 4188–4195. 10.1152/jn.00378.2005.

70. Taulu, S., and Simola, J. (2006). Spatiotemporal signal space separation method for rejecting nearby interference in MEG measurements. Phys Med Biol *51*, 1759–1768. 10.1088/0031-9155/51/7/008.

SUPPLEMENTARY INFORMATION

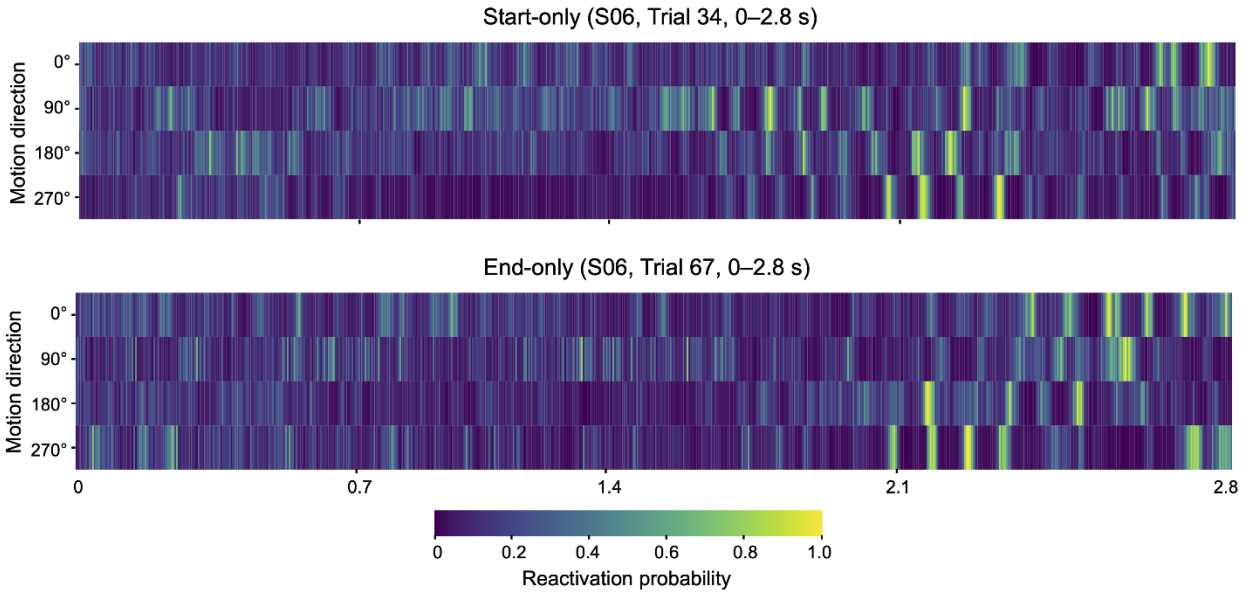

Figure S1. Decoded feature representations in start- and end-only conditions (related to Figures 2 and 3)

Time series of reactivation probability output from the four regression models on an example trial. Time zero corresponds to trial onset.

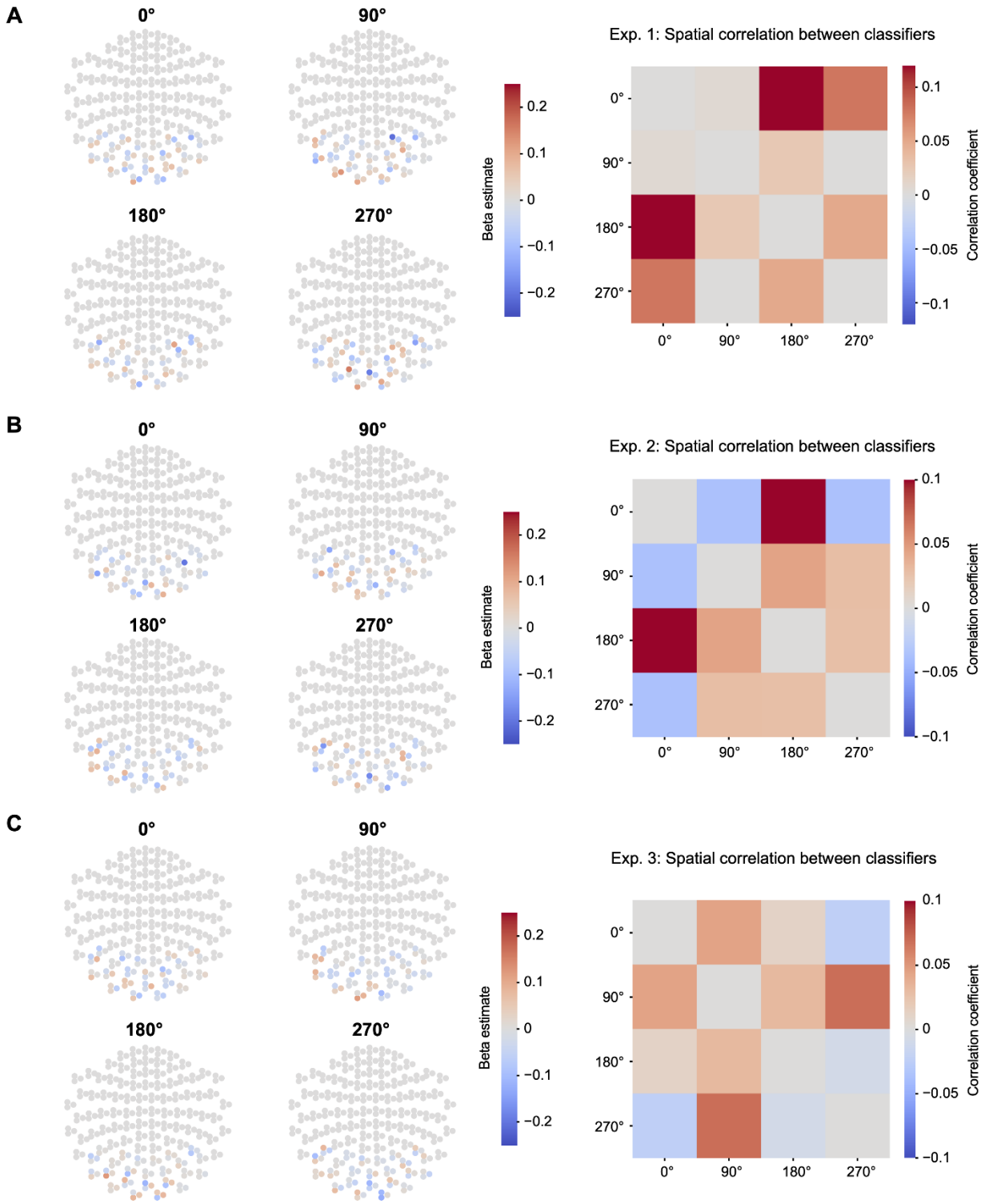

Figure S2. Sensor maps and spatial correlation of trained Lasso logistic regression models (related to Figure 1)

(A) Left: Sensor map for each state decoding model in Experiment 1; MEG signals from only 72 occipital sensors were selected as features while training the classifier. Right: Correlation matrix among classifiers. No spatial correlation was found among trained classifiers (highest correlation; $r < 0.12$). **(B and C)** Same as (A), except the sensor maps and correlation matrix correspond to Experiments 2 (Panel B, highest correlation; $r < 0.1$) and 3 (Panel C, highest correlation; $r < 0.1$), respectively.

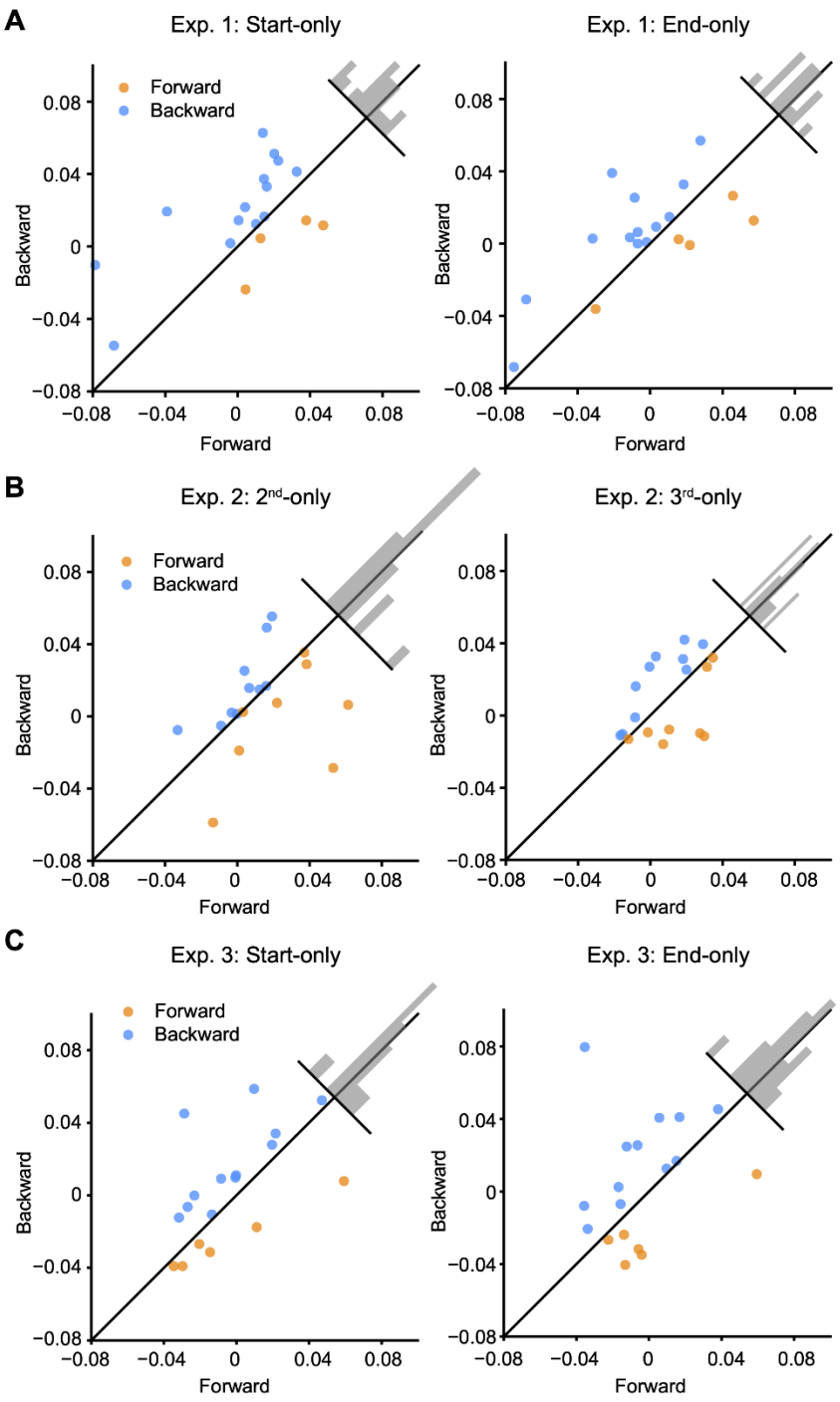

Figure S3. Sequenceness distribution across participants (related to Figures 3 and 4)

(A) In Experiment 1, of the 18 participants, 14 showed backward replay at 32 ms-lag for the start-only condition (left), and 13 showed backward replay at 32 ms-lag for the end-only condition (right). Each dot represents an individual participant. Backward and forward sequenceness is denoted by blue and yellow dots, respectively. The inset histogram shows the distribution of deviations from the unity line. **(B)** Same as described in (A), but for the results of Experiment 2 in the 2nd-only (left) and 3rd-only (right) conditions, respectively. **(C)** Same as described in (A) but for the results of Experiment 3 in the start-only (left) and end-only (right) conditions, respectively.

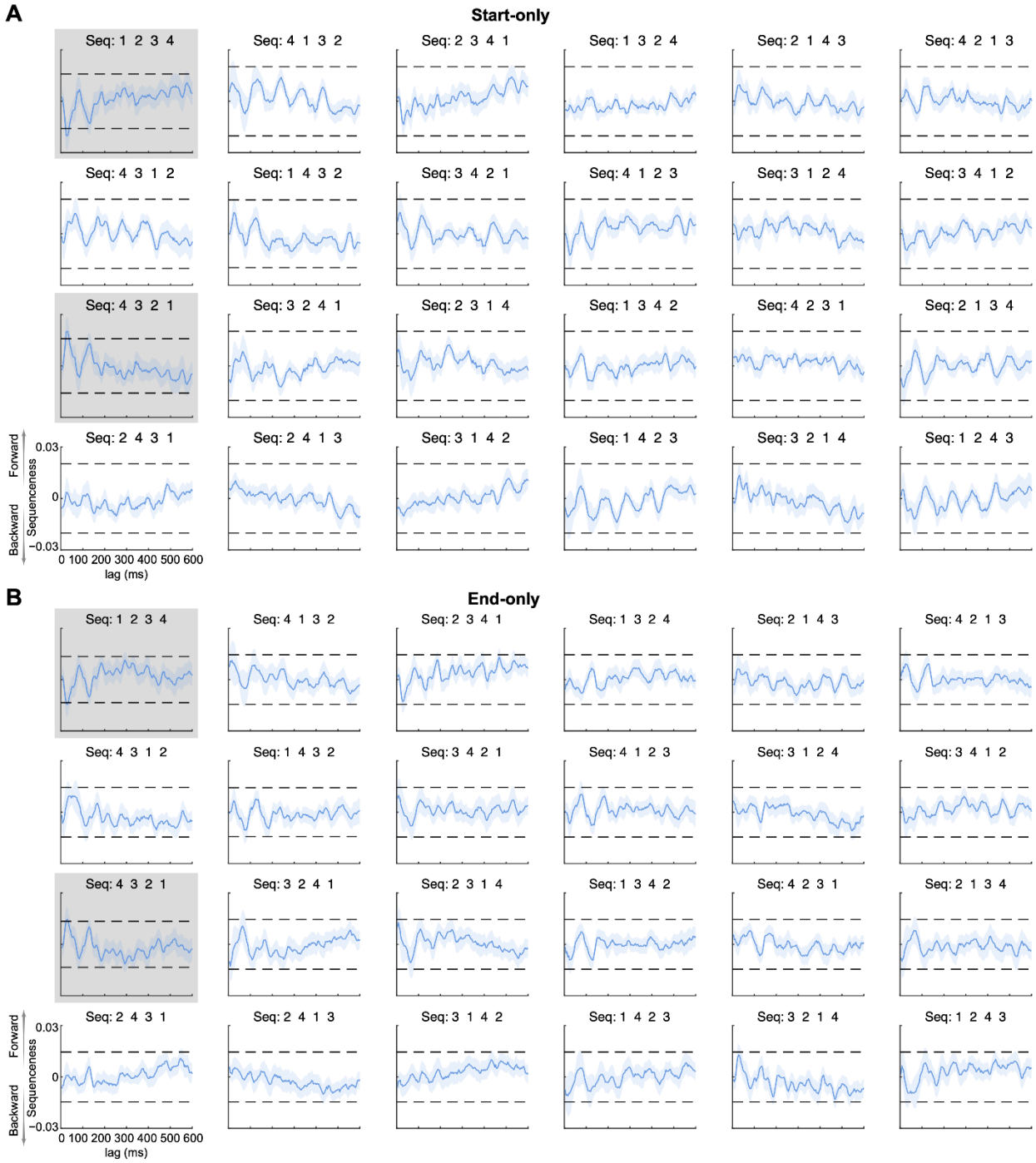

Figure S4. Sequenceness for each of the 24 possible orders (related to Figure 3)

(A) In the start-only condition of Experiment 1, only the backward sequence [4 → 3 → 2 → 1] with lags at 28–40 ms was significantly different (gray panels). The horizontal

dashed lines represent significance thresholds derived from state label permutation at the 2nd-level GLM matrix of temporally delayed linear modeling. **(B)** Same as described in (A) but for the end-only condition in Experiment 1.

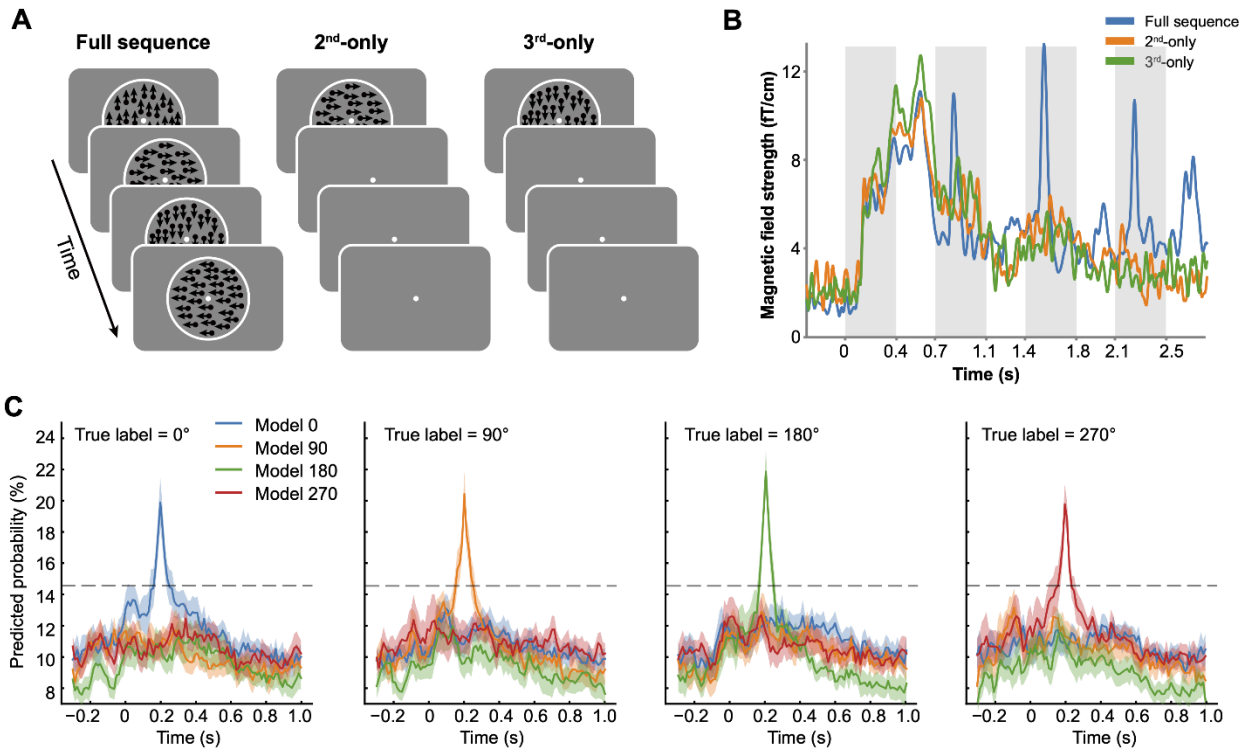

Figure S5. Stimuli, evoked responses, and classifier performance in Experiment 2 (related to Figure 4)

(A) Instead of the first or last RDK presented as a cue in Experiment 1, we presented the second (2nd-only condition) and third RDK (3rd-only condition) in Experiment 2. **(B)** Evoked responses as a function of time relative to trial onset during presentation of the full sequence (blue line), 2nd-only (yellow line), and 3rd-only (green line) conditions in Experiment 2, respectively. **(C)** We used a leave-one-out cross-validation procedure to assess each classifier in the functional localizer of Experiment 2. Each colored line indicates the predicted result of a different model at a different true state. The permutation threshold is indicated as a dashed horizontal line and was calculated by randomly shuffling the labels and re-decoding.

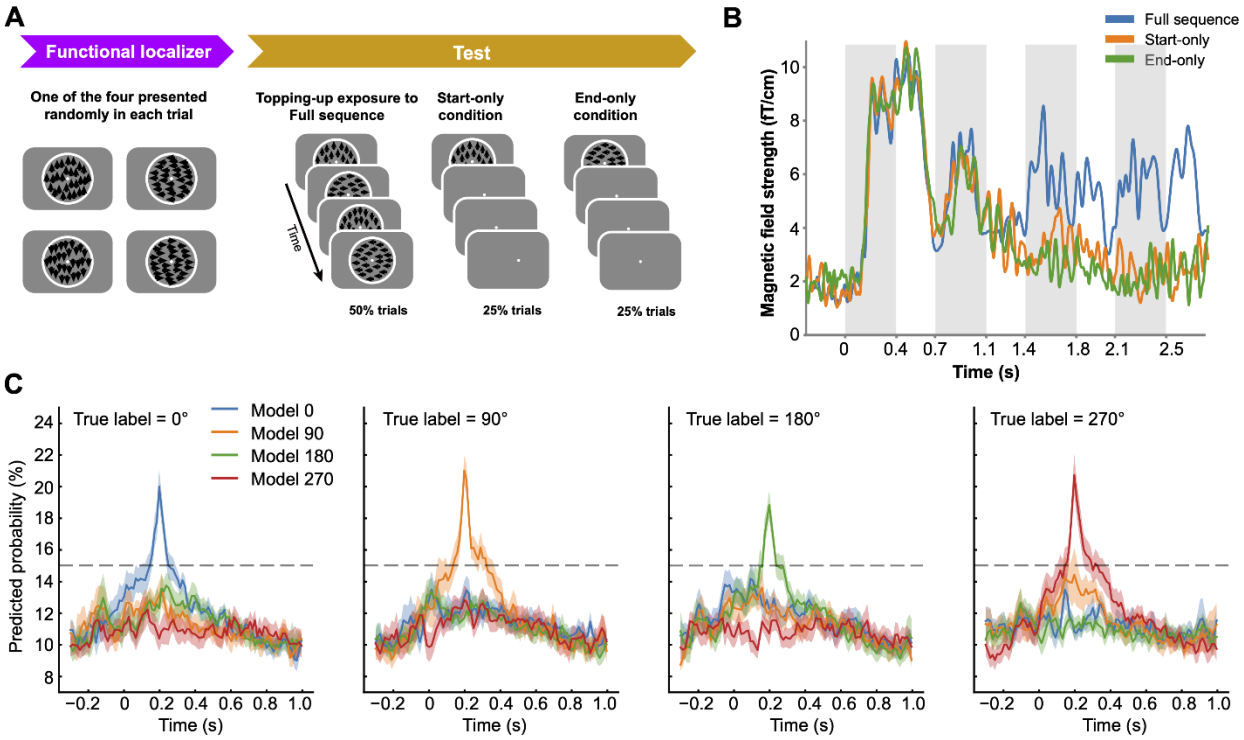

Figure S6. Experimental procedure, evoked responses, and classifier performances in Experiment 3 (related to Figure 4)

(A) All setups in Experiment 3 were identical to those of Experiment 1 except for removed pre-exposure. **(B)** Evoked responses as a function of time relative to trial onset during the presentation of the full sequence (blue line), start-only (yellow line), and end-only (green line) conditions in Experiment 3, respectively. **(C)** We used a leave-one-out cross-validation procedure to assess each classifier in the functional localizer of Experiment 3. Each colored line indicates the predicted result of a different model at a different true state. The permutation threshold is shown as a dashed horizontal line and was calculated by randomly shuffling the labels and re-decoding.